Hund Physics Landscape of Two-Orbital Systems

Siheon Ryee,[1] Myung Joon Han,[1,*] and Sangkook Choi[2,†]
[1]Department of Physics, KAIST, Daejeon 34141, Republic of Korea
[2]Condensed Matter Physics and Materials Science Department, Brookhaven National Laboratory, Upton, New York 11973, USA

(Received 30 August 2020; revised 10 February 2021; accepted 29 March 2021; published 17 May 2021)

Motivated by the recent discovery of superconductivity in infinite-layer nickelates $RE_{1-\delta}Sr_{\delta}NiO_2$ (RE = Nd, Pr), we study the role of Hund coupling J in a quarter-filled two-orbital Hubbard model, which has been on the periphery of the attention. A region of negative effective Coulomb interaction of this model is revealed to be differentiated from three- and five-orbital models in their typical Hund metal active fillings. We identify distinctive regimes including four different correlated metals, one of which stems from the proximity to a Mott insulator, while the other three, which we call "intermediate" metal, weak Hund metal, and valence-skipping metal, from the effect of J being away from Mottness. Defining criteria characterizing these metals is suggested, establishing the existence of Hund metallicity in two-orbital systems.

DOI: 10.1103/PhysRevLett.126.206401

A novel route to the electron correlation, which has attracted a great deal of attention over the last fifteen years, is on-site Hund coupling J [1]. This energy scale favors high-spin configurations on each atom, lifting the degeneracy of atomic multiplets. In multiorbital systems away from half filling, an intriguing correlated metallic regime dubbed Hund metal emerges, promoted by J rather than the proximity to a Mott insulator [1–4]. Accordingly, many related physical phenomena have been uncovered, such as the spin-freezing crossover [5,6], the spin-orbital separation [7–13], instability to the charge disproportionation [14,15], the orbital differentiation [16–22], and superconductivity [6,23], to name a few. These concepts have provided a compelling view of the physics, most prominently of iron-based superconductors [2,3,18,19,23–29] and ruthenates [30–33].

In the midst of unveiling Hund metal phenomenology, however, two-orbital models with one electron away from half filling have been on the periphery of the attention, although intriguing effects of Hund coupling have been reported [4,17,34]. This is presumably because this usual filling for Hund metallicity results in the seemingly trivial singly occupied electron or hole state for this case.

The recent discovery of the superconductivity in infinite-layer nickelates $RE_{1-\delta}Sr_{\delta}NiO_2$ (RE = Nd, Pr) [35,36] heralds a new chapter of quantum materials research [37–70]. Despite their chemical and structural similarities with cuprates (nominal one-hole occupation of Ni-d orbitals residing in the NiO_2 plane), they exhibit sharp differences in their normal state physical properties. Most strikingly, they are metals without long-range magnetic orders showing non-Fermi-liquid behaviors at elevated temperatures [35,36,71,72]. A series of the recent *ab initio* studies reported the importance of Hund coupling [65–69], especially among Ni-e_g (two-orbital) electrons [68], alluding to an intriguing route to the superconductivity [49–51]. Although these observations are interesting *per se*, a suitable reference picture of Hund physics has yet to be established.

To that end, in this Letter we classify distinctive regimes emerging out of a two-orbital Hubbard model away from half filling. Four different correlated metals are identified: one of which stems from the proximity to a Mott insulator, while the other three result from effects of J being away from Mottness. The latter three J-induced metals are intermediate, weak Hund (WH), and valence-skipping (VS) metals. Characteristic features of these metals will be discussed throughout the Letter. We finally discuss implications of our two-orbital picture to the physics of infinite-layer nickelates.

To obtain a basic picture, we first begin with a brief excursion into a simple atomic limit: a collection of atoms with zero hopping among them. We consider three different models: two-, three-, and five-orbital models with $n_d = M + 1$ electron filling (where M is the number of orbitals). This particular choice is motivated by the observation that a system with $n_d = M \pm 1$ hosts Hund metallicity when they form solids (at the least for $M \geq 3$), as well as that each model is relevant to nickelates ($M = 2$), ruthenates ($M = 3$), and iron-based superconductors ($M = 5$). We take the following form for the local Hamiltonian of $M = 2$ and 3 models:

$$H_{\mathrm{loc}} = U\sum_{m} n_{m\uparrow}n_{m\downarrow} + \sum_{mm',\sigma\sigma'}^{m<m'} (U' - J\delta_{\sigma\sigma'})n_{m\sigma}n_{m'\sigma'} + J\sum_{mm'}^{m\neq m'} (d^{\dagger}_{m\uparrow}d^{\dagger}_{m'\downarrow}d_{m\downarrow}d_{m'\uparrow} + d^{\dagger}_{m\uparrow}d^{\dagger}_{m\downarrow}d_{m'\downarrow}d_{m'\uparrow}) - \mu\sum_{m,\sigma} n_{m\sigma}, \quad (1)$$

where $d^{\dagger}_{m\sigma}$ ($d_{m\sigma}$) is the electron creation (annihilation) operator with orbital index $m = 1, \ldots, M$ and spin index $\sigma = \uparrow, \downarrow$. $n_{m\sigma} = d^{\dagger}_{m\sigma} d_{m\sigma}$ is the number operator. μ is the chemical potential to obey average electron filling of $n_d = M + 1$ per site. U (U') is intraorbital (interorbital) Coulomb energy cost. We set $U' = U - 2J$ assuming cubic symmetry. For the $M = 5$ case, the above Kanamori-type two-body terms are far from reality, and thus a well-suited strategy, e.g., Slater parametrization, is required. One possible way is to introduce the relative strength of anisotropic interaction ($1/\gamma$ where $\gamma > 0$) and reparametrize Slater integrals in terms of it [73]. In this way, $1/\gamma = 0$ limit corresponds to Eq. (1) even for $M = 5$ (see Supplemental Material [74], which includes Refs. [75,76]).

The ground state configurations of atomic limit at vanishing temperature ($T = 0$) are presented in Fig. 1. Here we use notation cd^n to denote the ratio (c) of sites having n-electron occupation in the configuration. The homogeneous phases (d^{n_d}) occupy the small J/U regions relevant to most of real materials.

For large J/U, on the other hand, the mixed valence phases emerge. For all the cases with Kanamori interaction ($1/\gamma = 0$ for $M = 5$), the transition occurs from a homogeneous to a mixed valence state when $J/U > 1/3$, i.e., $U - 3J < 0$. Only the $M = 2$ case shows VS transition $[d^N \to (d^{(N+1)} + d^{(N-1)})/2]$ under this form of interaction. This VS phenomenon is the direct manifestation of the negative U_{eff}: $U_{\mathrm{eff}} \equiv E_{N+1} + E_{N-1} - 2E_N < 0$, where E_N is the energy of the lowest-lying N-electron state [77–79]. The $1/\gamma \neq 0$ case of $M = 5$ also leads to VS, albeit an extreme form of mixed valence preempts the region of $J/U > 1/(3 + 2/\gamma)$ masking the VS phase (see the rightmost panel in Fig. 1 or see Ref. [73] for the $M = 5$ case). To summarize, we identify $M = 2$ case as the *minimal* model for J-driven VS phenomenon.

With insight obtained above, we now turn to the actual lattice problem with nonzero hopping. In order to focus on generic features rather than material specific ones, we consider the infinite-dimensional Bethe lattice of semicircular density of states with half-bandwidth $D = 1$. D is hereafter used as the unit of energy. We solve the $M = 2$ case with $n_d = 3$ (particle-hole symmetric about $N = 2$). The interaction form of Eq. (1) is used for nonhybridized degenerate two orbitals. The model is solved within the dynamical mean-field theory (DMFT) [80] employing COMCTQMC implementation [81] of the hybridization-expansion continuous-time quantum Monte Carlo algorithm [82] as an impurity solver. Unless otherwise specified, $T = 0.01$. We restrict ourselves to paramagnetic solutions without spatial symmetry breaking.

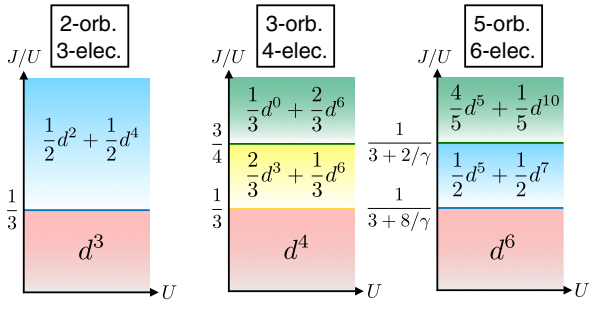

FIG. 1. Atomic limit phase diagrams at $T = 0$, $U > 0$, and $J/U \geq 0$ for three different models ($M = 2$, 3, and 5 systems) with $n_d = M + 1$. The lowest-energy configurations are indicated at each region. The VS phase is highlighted in the sky blue region.

The central physical quantity of the present study is the onset temperatures of screening of spin and orbital degrees of freedom. These two temperatures, $T^{\mathrm{onset}}_{\mathrm{spin}}$ and $T^{\mathrm{onset}}_{\mathrm{orb}}$, are defined as the temperature below which the Curie law of the unscreened local spin and orbital moments starts to become violated and screening sets in [12]. A hallmark of strong Hundness is the separation of these two temperatures: $T^{\mathrm{onset}}_{\mathrm{orb}} \gg T^{\mathrm{onset}}_{\mathrm{spin}}$ yielding a range of temperature in which the unscreened local spin moment coexists with the screened orbital degrees of freedom [7–13,83]. We will measure the separation of two T^{onset} as $\Delta T^{\mathrm{onset}} \equiv T^{\mathrm{onset}}_{\mathrm{orb}} - T^{\mathrm{onset}}_{\mathrm{spin}}$. To locate the onset temperatures, we first evaluate the local spin and orbital susceptibilities: $\chi_{\mathrm{s/o}} = \int_0^{1/T} d\tau (\langle O_{\mathrm{s/o}}(\tau) O_{\mathrm{s/o}} \rangle - \langle O_{\mathrm{s/o}} \rangle^2)$, where $O_{\mathrm{s}}(\tau) = \sum_m n_{m\uparrow}(\tau) - n_{m\downarrow}(\tau)$ for spin and $O_{\mathrm{o}}(\tau) = \sum_\sigma n_{1\sigma}(\tau) - n_{2\sigma}(\tau)$ for orbital (τ = imaginary time) up to $T = 1$, and then fit high-T data to the following formula: $\chi_{\mathrm{s/o}} \propto 1/(T + T^{\mathrm{onset}}_{\mathrm{spin/orb}})$.

Figure 2(a) presents our calculated $\Delta T^{\mathrm{onset}}$ as a function of U_{eff}. Most interestingly, we found a *generic* scaling relation between $\Delta T^{\mathrm{onset}}$ and U_{eff}. Note also that $T^{\mathrm{onset}}_{\mathrm{orb}}/T^{\mathrm{onset}}_{\mathrm{spin}}$ clearly shows the same trend as shown in the inset of Fig. 2(a). This implies that U_{eff} ($U_{\mathrm{eff}} = U - 3J$ for our case) is the crucial factor, rather than U or J alone, for the separation of two onset temperatures. This result is consistent with the recent comparative study of real materials [12] and demonstrates the generality holding for a wide range of U and J/U in the two-orbital model.

By looking at Fig. 2(a), one can first notice the presence of two distinctive types of insulators, namely the Mott and valence-skipping insulators at large positive and negative values of U_{eff}, respectively. The former is the result of suppressed charge fluctuations localizing electron motions, thereby maximizing the probability of $|N = n_d = 3, S = 1/2\rangle$ multiplets (N = charge, S = spin). By contrast, the latter form of insulator exhibits the predominance of two multiplets, $|2, 1\rangle$ and $|4, 0\rangle$, with largely suppressed $|3, 1/2\rangle$ probability because $U_{\mathrm{eff}} < 0$ [74]. The presence of these two phases is reminiscent of the atomic limit result (see Fig. 1).

Interestingly, we identify distinctive regimes within the metallic phase intervening between the two insulators. When $U \gg J$, a metal with $\Delta T^{\mathrm{onset}} \simeq 0$ is found to appear

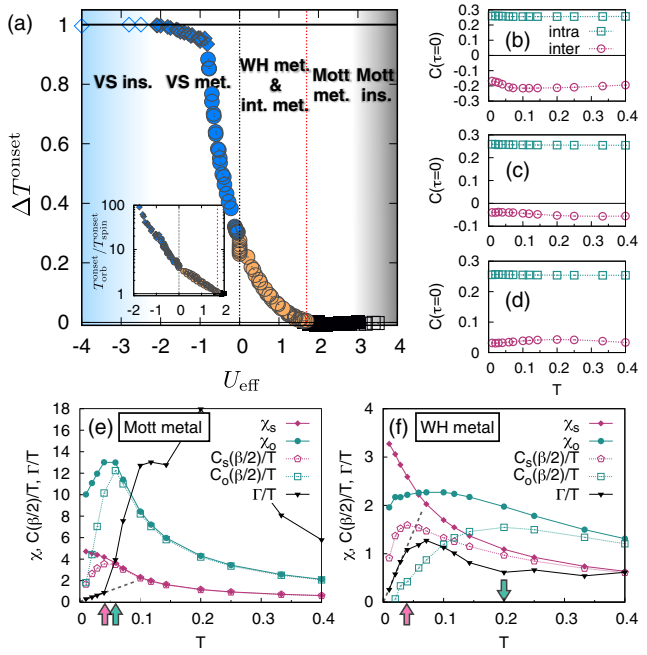

FIG. 2. (a) $\Delta T^{\rm onset}$ as a function of $U_{\rm eff}$ obtained from $2 \le U/D \le 8$ and $0 \le J/U \le 0.5$. The red dotted line indicates the approximate value of $U_{\rm eff}$ below which $\Delta T^{\rm onset} > 0$. The black dotted line denotes $U_{\rm eff} = 0$. We used $T = 0.05$ to stabilize the VS insulator phase [84]. The diamond symbols denote the region in which $T^{\rm onset}_{\rm orb} > 1$. Inset: $T^{\rm onset}_{\rm orb}/T^{\rm onset}_{\rm spin}$ as a function of $U_{\rm eff}$. (b)–(d) $C_{\rm intra}$ (green square) and $C_{\rm inter}$ (magenta circle) at $U = 4$ for (b) Mott metal ($J/U = 0.15$; $U_{\rm eff} = 2.2$), (c) WH metal ($J/U = 0.3$; $U_{\rm eff} = 0.4$), and (d) VS metal ($J/U = 0.37$; $U_{\rm eff} = -0.44$). (e)–(f) $\chi_{s/o}$, Γ/T, and $C_{s/o}(\beta/2)/T$ plotted as a function of T at $U = 4$ for (e) Mott metal ($J/U = 0.15$; $U_{\rm eff} = 2.2$) and (f) WH metal ($J/U = 0.3$; $U_{\rm eff} = 0.4$). $T^{\rm peak}_{\rm spin/orb}$ are marked with magenta (spin) and green (orbital) arrows. The gray dashed lines are guides to the eye to indicate quasilinearity of Γ/T (i.e., $\Gamma \sim T^2$).

near a Mott insulator where Mottness dominates over Hundness [see Fig. 2(a)]. To gain some understanding of this behavior, we resort to a low-energy Kondo model by performing a Schrieffer-Wolff transformation of relevant impurity Hamiltonian [85]. The resulting Kondo coupling constants ($\mathcal{J}^i$) when $U > J$ read $\mathcal{J}^i_{U,J} \simeq \mathcal{J}^i_{U,J=0} + \mathcal{O}(J/U^2) + \mathcal{O}(J^2/U^3) + \cdots$ because $\mathcal{J}^i_{U,J} \sim V^2/\Delta E$. Here, V is the bath-impurity hybridization strength and ΔE is the charge excitation energy from $N = n_d$ to $N = n_d \pm 1$ subspaces. In the regime of $U \gg J$, $\mathcal{J}^i_{U,J} \simeq \mathcal{J}^i_{U,J=0}$ by which the system approximates to a SU(4) model having $\mathcal{J}^{\rm spin} = \mathcal{J}^{\rm orb}$. In this case, the relation $\mathcal{J}^{\rm spin} = \mathcal{J}^{\rm orb}$ also holds under renormalization group flow [10,86]; thereby the Kondo screening of spin and orbital occur simultaneously. In this respect, we identify a regime of strong Mottness ($U \gg J$) with $\Delta T^{\rm onset} \simeq 0$. Following the terminology of Refs. [12,13], we call the metallic regime of $\Delta T^{\rm onset} \simeq 0$ a Mott metal [see Fig. 2(a)].

On the contrary, there exist metals with a finite $\Delta T^{\rm onset}$. Near the VS insulator, where $U_{\rm eff} < 0$, a correlated metal emerges exhibiting a tendency of valence skipping, which we call a VS metal [Fig. 2(a)]. In order to characterize this metal, we examine the sign of $C_{\rm inter}$ ($C_{\rm intra/inter} = \langle \delta n_m \delta n_{m'} \rangle$ where $\delta n_m = \sum_\sigma n_{m\sigma} - \langle \sum_\sigma n_{m\sigma} \rangle$ and $m \neq m'$ for $C_{\rm inter}$, while $m = m'$ for $C_{\rm intra}$). As VS metal emerges when $U_{\rm eff} < 0$, multiplets in $N = 2$ and $N = 4$ charge subspaces are lower in energy than those of $N = 3$. Thus, either electrons or holes try to occupy both orbitals, yielding $C_{\rm inter} > 0$ in contrast to the case of metals belonging to $U_{\rm eff} > 0$ [compare Fig. 2(d) with Figs. 2(b) and 2(c)]. Because of this negativity of $U_{\rm eff}$, the VS region is highly susceptible to the formation of charge disproportionation [15,73] or superconductivity [6,87], thereby being detectable when accompanied by such orders.

We now turn to the metallic region where $U_{\rm eff} > 0$ with $\Delta T^{\rm onset} > 0$, which is of particular interest to us due to the potential presence of Hund metallicity. Although strong Hundness is argued to be manifested by $\Delta T^{\rm onset} > 0$ [12], the presence of Hund metal regime in our two-orbital model has yet to be established. The emergence of Hund metallicity has been attributed to the two-faced effect of J dubbed the "Janus effect" suppressing the quasiparticle weight Z [88] on one hand, while enhancing U_c (U_c = the critical value of U for the Mott transition) on the other hand [4]. Thereby it reflects the stronger correlation (i.e., reduced Z) induced by J rather than the proximity to a Mott insulator. This effect has been clearly seen in systems with $n_d = M \pm 1$ among $M \ge 3$ orbitals in which the atomic ground state degeneracy is lifted by J [1,4]. On the contrary, our two-orbital system with $n_d = M + 1 = 3$ hosts a single hole, whereby it has been a conventional wisdom that the Janus effect is absent in two-orbital models.

Here we argue that, albeit weak, the Janus effect can be identified even in the two-orbital case. We first note that the conventional way of capturing this effect is to plot the evolution of Z as a function of U, and then to examine whether the suppression of Z and enhancement of U_c simultaneously occur at a fixed U as J is increased, i.e., examining whether $(\partial Z/\partial J)_U < 0$ and $dU_c(J)/dJ > 0$. In this strategy, however, the interorbital Coulomb energy cost, $U' = U - 2J$, is not fixed as J is varied. Thus, the genuine effect of tuning J is partly masked by the reduced U'.

To circumvent the above difficulty, we propose an alternative "gauge" of measuring the Janus effect: examining the sign of $(\partial Z/\partial J)_{U_{\rm av}}$, where $U_{\rm av} \equiv 1/M^2 \sum_{mm'} \mathcal{U}_{mm'}$ ($\mathcal{U}_{mm'}$ = elements of Coulomb interaction tensor; see Supplemental Material [74]). The rationale behind this proposal is that one should count not only the intraorbital ($m = m'$), but also the interorbital ($m \neq m'$) Coulomb energy cost, which may vary with J. For the current $M = 2$ case, $U_{\rm av} = U - J$. It is worth noting that within

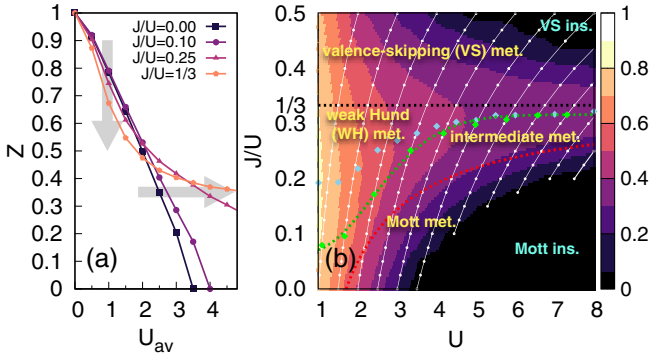

(c)

	$U_{\rm eff}$	$C_{\rm inter}$	$\Delta T^{\rm onset}$	$dU_c(J)/dJ$	$\partial Z/\partial J$
Mott met.	+	−	$\simeq 0$	+	+
inter. met.	+	−	+	+	+
WH met.	+	−	+	+	−
VS met.	−	+	+	+	−

FIG. 3. (a) Z as a function of $U_{\rm av}(=U-J)$ for several $J/U[=(J/U_{\rm av})/(1+J/U_{\rm av})]$. (b) Phase diagram with color scheme representing Z. The red and black dotted lines indicate the same as in Fig. 2(a). The green dotted line is an estimated boundary of J/U above which the Janus effect emerges: $(\partial Z/\partial J)_{U_{\rm av}}<0$, while $dU_c(J)/dJ>0$. Green diamonds are actual crossing points where $(\partial Z/\partial J)_{U_{\rm av}}=0$, whereas blue ones are $(\partial Z/\partial J)_U=0$ plotted for comparison. A set of U and J/U values belonging to the same $U_{\rm av}$ are connected with a white solid line. (c) Characteristic features of different correlated metals. Here, $+/-$ denote the sign of the corresponding quantity.

the Slater parametrization for $M=5$, $U_{\rm av}=F^0$ ($F^0=$ the zeroth-order Slater integral, which is the monopole term of Coulomb interaction). We also point out that this kind of viewpoint is implicitly embodied in some *ab initio* studies (e.g., Refs. [2,67]) by the use of Slater parametrization of the Coulomb interaction with F^0 remaining unchanged while varying J in searching for the Hund physics. With this idea in mind, we plot Z vs $U_{\rm av}$ in Fig. 3(a). One can now clearly capture the Janus effect; namely, $(\partial Z/\partial J)_{U_{\rm av}}<0$ and $dU_c(J)/dJ>0$. We suspect that this reduction of Z by J is attributed to the lifted degeneracy in $N=2$ (half-filling) charge subspace. In this subspace, J elevates the energy of $|2,0\rangle$ states and lowers that of $|2,1\rangle$. The enhanced fluctuation between $|2,1\rangle$ and $|3,1/2\rangle$ suppresses Fermi liquid coherence as in the case of $M\geq 3$ models with $n_d=M\pm 1$ [3,8–10]. In the meanwhile, the atomic state of n_d subspace ($N=3$) is not affected by J since it plays no role when a single electron or hole is occupied. As a result, overall influence of J is weaker than the $M\geq 3$ cases. In this sense, we call our metallic regime satisfying $(\partial Z/\partial J)_{U_{\rm av}}<0$ [or $(\partial Z/\partial J)_U<0$] and $dU_c(J)/dJ>0$ a "weak" Hund metal [Fig. 3(b)].

As a central result of our Letter, we present the phase diagram exhibiting different metallic regimes; see Fig. 3(b). In Fig. 3(c), we also summarize characteristic features of these correlated metals. The green dotted line in Fig. 3(b) denotes J/U above which the Janus effect exists. Hence we now further classify the region of $U_{\rm eff}>0$ and $\Delta T^{\rm onset}>0$ into two: WH metal exhibiting the Janus effect and intermediate metal, which emerges in an intermediate region between the WH and Mott metals. In the intermediate metal, J alleviates the correlation strength, i.e., $(\partial Z/\partial J)_{U_{\rm av}}>0$, although spin-orbital separation ($\Delta T^{\rm onset}>0$) occurs.

A notable feature of this phase diagram is that near the $J/U=1/3$ line, which is the boundary between WH and VS metals, the quasiparticle survives up to an arbitrarily large U. Indeed, $(\partial Z/\partial U_{\rm av})_{J/U=1/3}\to 0$, while Z remains small but finite as $U_{\rm av}$ is increased [Fig. 3(a)]. This is because the lowest-energy atomic multiplets in $N=n_d$ and $N=n_d\pm 1$ subspaces are degenerate or sufficiently close in energy around this line, resulting in $U_{\rm eff}=U-3J\simeq 0$. As a result, hopping processes become feasible, which otherwise should be blocked due to a large Coulomb energy cost [14].

Having established an overall picture, we now further examine the spin-orbital separation via long-time spin and orbital correlators at $\tau=\beta/2$ ($\beta=1/T$): $C_{\rm s/o}(\beta/2)=\langle O_{\rm s/o}(\beta/2)O_{\rm s/o}\rangle-\langle O_{\rm s/o}\rangle^2$ in Figs. 2(e) and 2(f). At sufficiently low temperatures, $C_{\rm s/o}(\beta/2)$ scales as $C_{\rm s/o}(\beta/2)\sim\{T/[\sin(\pi/2)]\}^\alpha$ with $\alpha=2$ in a Fermi liquid, while $\alpha=1$ in the crossover between local moment and the Fermi liquid [5,89]. In the unscreened local moment regime, $C_{\rm s/o}(\beta/2)$ is basically T independent and $\chi_{\rm s/o}\simeq C_{\rm s/o}(\beta/2)/T$ [Figs. 2(e) and 2(f)]. In light of this observation, we investigate $C_{\rm s/o}(\beta/2)/T$ for an extended range of T. These quantities should be T linear in the Fermi liquid, whereas scale as $1/T$ in the local moment regime. As a consequence, a narrow region of crossover between these two emerges, forming a hump of $C_{\rm s/o}(\beta/2)/T$. Temperatures at which peaks of $C_{\rm s/o}(\beta/2)/T$ appear ($T^{\rm peak}_{\rm spin/orb}$) are marked with arrows in Figs. 2(e) and 2(f). One can clearly notice that the $T^{\rm peak}_{\rm spin}$ coincides with $T^{\rm peak}_{\rm orb}$ in the Mott metal, whereas two crossover temperatures become separated in the metals with finite $\Delta T^{\rm onset}$, such as WH metal. Furthermore, below $T^{\rm peak}_{\rm spin}$, the quasiparticle scattering rate $\Gamma=-Z{\rm Im}[\Sigma(i\omega)]|_{\omega\to 0}$ roughly follows the Fermi-liquid behavior ($\Gamma\propto T^2$). This result is consistent with the observation that $C_{\rm s}(\beta/2)/T$ is sublinear in T when $T<T^{\rm peak}_{\rm spin}$.

While we mainly focus on the generic features of Mott and Hund physics, its relevance to $RE_{1-\delta}Sr_\delta NiO_2$ is of particular interest. Our two orbitals can be regarded as Ni-$d_{x^2-y^2}$ and another Ni-d orbital. *Ab initio* estimate of Coulomb interaction for a Ni-e_g model reads $U/D\simeq 1.7$ and $J/U\simeq 0.2$ [40], which falls into the WH metal region [Fig. 3(b)]. However, Δ, the on-site energy level splitting between two orbitals, and its competition with J should

also be taken into account. If Δ dominates over J, singlet $|2,0\rangle$ would be favored over triplet $|2,1\rangle$, hampering strong Hund physics. In the presence of Δ, eigenvalues of the local Hamiltonian are $E_{|2,0\rangle} = U - \Delta - \sqrt{J^2 + \Delta^2} - 2\mu$ and $E_{|2,1\rangle} = U - 3J - \Delta - 2\mu$ for $|2,0\rangle$ and $|2,1\rangle$, respectively [74]. Hence, the criterion for predominance of $|2,1\rangle$ over $|2,0\rangle$ (i.e., $E_{|2,1\rangle} < E_{|2,0\rangle}$) is $J/\Delta > \sqrt{2}/4 \simeq 0.354$. However, the estimated value $J/\Delta \simeq 0.3$ for $Nd_{0.8}Sr_{0.2}NiO_2$ between two Ni-e_g [40,65] is slightly smaller than the "bare" critical value $J/\Delta \simeq 0.354$. In this respect, nickelates may belong to the competing region where large J/U favors Hund metallicity, while J/Δ, which is slightly smaller than its threshold value, refrains from forming high spin in the two-hole atomic state (see Supplemental Material for related DMFT results [74]). Thus, the metallic nature of doped nickelates are sensitive to the small changes in J/Δ. Interestingly, indeed, a recent full-band *ab initio* study reports higher weight of $|2,1\rangle$ than $|2,0\rangle$ [68], indicating the effective enhancement of J/Δ. Further studies are highly desirable to confirm our picture.

To conclude, we have identified distinctive correlated metal regimes emerging out of the two-orbital Hubbard model at quarter filling. This simple model is revealed to be differentiated from three- as well as five-orbital models in their Hund metal active fillings, showing the transition to the VS phases. We found a generic scaling relation between the degree of spin-orbital separation (ΔT^{onset}) and U_{eff} and established a weak Hund metal behavior in which J enhances the correlation strength. We also discussed the implications of our two-orbital picture for the nature of the metallic state of $RE_{1-\delta}Sr_\delta NiO_2$. We also remark that, in this multiorbital viewpoint on nickelates, the role of nonlocal correlations and interactions and the emergence of symmetry-broken phases [6,15,27,28,90–93] are intriguing open problems. In addition to $RE_{1-\delta}Sr_\delta NiO_2$, the low-energy physics of $RNiO_3$ (R = rare-Earth elements) is reported to be well described by Ni-e_g bands [94,95]. Thus, a series of analyses presented in this study should also provide useful insights to these compounds.

S. R. and M. J. H. were supported by Creative Materials Discovery Program through NRF (2018M3D1A1058754) and Basic Science Research Program (2018R1A2B-2005204). S. C. was supported by the U.S. Department of Energy, Office of Science, Basic Energy Sciences as a part of the Computational Materials Science Program. This research used resources of the National Energy Research Scientific Computing Center (NERSC), a U.S. Department of Energy Office of Science User Facility operated under Contract No. DE-AC02-05CH11231.

*mj.han@kaist.ac.kr
†sachoi@bnl.gov

[1] A. Georges, L. de Medici, and J. Mravlje, Annu. Rev. Condens. Matter Phys. **4**, 137 (2013).
[2] K. Haule and G. Kotliar, New J. Phys. **11**, 025021 (2009).
[3] Z. Yin, K. Haule, and G. Kotliar, Nat. Mater. **10**, 932 (2011).
[4] L. de' Medici, J. Mravlje, and A. Georges, Phys. Rev. Lett. **107**, 256401 (2011).
[5] P. Werner, E. Gull, M. Troyer, and A. J. Millis, Phys. Rev. Lett. **101**, 166405 (2008).
[6] S. Hoshino and P. Werner, Phys. Rev. Lett. **115**, 247001 (2015).
[7] K. M. Stadler, Z. P. Yin, J. von Delft, G. Kotliar, and A. Weichselbaum, Phys. Rev. Lett. **115**, 136401 (2015).
[8] Z. P. Yin, K. Haule, and G. Kotliar, Phys. Rev. B **86**, 195141 (2012).
[9] A. Horvat, R. Žitko, and J. Mravlje, Phys. Rev. B **94**, 165140 (2016).
[10] C. Aron and G. Kotliar, Phys. Rev. B **91**, 041110(R) (2015).
[11] A. Horvat, R. Zitko, and J. Mravlje, arXiv:1907.07100.
[12] X. Deng, K. M. Stadler, K. Haule, A. Weichselbaum, J. von Delft, and G. Kotliar, Nat. Commun. **10**, 2721 (2019).
[13] K. Stadler, G. Kotliar, A. Weichselbaum, and J. von Delft, Ann. Phys. (Amsterdam) **405**, 365 (2019).
[14] A. Isidori, M. Berović, L. Fanfarillo, L. de' Medici, M. Fabrizio, and M. Capone, Phys. Rev. Lett. **122**, 186401 (2019).
[15] S. Ryee, P. Sémon, M. J. Han, and S. Choi, npj Quantum Mater. **5**, 19 (2020).
[16] L. de' Medici, S. R. Hassan, M. Capone, and X. Dai, Phys. Rev. Lett. **102**, 126401 (2009).
[17] L. de' Medici, Phys. Rev. B **83**, 205112 (2011).
[18] E. Bascones, B. Valenzuela, and M. J. Calderón, Phys. Rev. B **86**, 174508 (2012).
[19] N. Lanatà, H. U. R. Strand, G. Giovannetti, B. Hellsing, L. de' Medici, and M. Capone, Phys. Rev. B **87**, 045122 (2013).
[20] L. de' Medici, G. Giovannetti, and M. Capone, Phys. Rev. Lett. **112**, 177001 (2014).
[21] A. Kostin, P. O. Sprau, A. Kreisel, Y. X. Chong, A. E. Böhmer, P. C. Canfield, P. J. Hirschfeld, B. M. Andersen, and J. S. Davis, Nat. Mater. **17**, 869 (2018).
[22] F. B. Kugler, Seung-Sup B. Lee, A. Weichselbaum, G. Kotliar, and J. von Delft, Phys. Rev. B **100**, 115159 (2019).
[23] T.-H. Lee, A. Chubukov, H. Miao, and G. Kotliar, Phys. Rev. Lett. **121**, 187003 (2018).
[24] P. Hansmann, R. Arita, A. Toschi, S. Sakai, G. Sangiovanni, and K. Held, Phys. Rev. Lett. **104**, 197002 (2010).
[25] Z. Yin, K. Haule, and G. Kotliar, Nat. Phys. **7**, 294 (2011).
[26] L. Fanfarillo, G. Giovannetti, M. Capone, and E. Bascones, Phys. Rev. B **95**, 144511 (2017).
[27] L. de' Medici, Phys. Rev. Lett. **118**, 167003 (2017).
[28] P. Villar Arribi and L. de' Medici, Phys. Rev. Lett. **121**, 197001 (2018).
[29] A. S. Belozerov, A. A. Katanin, and V. I. Anisimov, Phys. Rev. B **97**, 115141 (2018).
[30] J. Mravlje, M. Aichhorn, T. Miyake, K. Haule, G. Kotliar, and A. Georges, Phys. Rev. Lett. **106**, 096401 (2011).
[31] J. Mravlje and A. Georges, Phys. Rev. Lett. **117**, 036401 (2016).
[32] F. B. Kugler, M. Zingl, H. U. R. Strand, Seung-Sup B. Lee, J. von Delft, and A. Georges, Phys. Rev. Lett. **124**, 016401 (2020).

[33] H. J. Lee, C. H. Kim, and A. Go, Phys. Rev. B **102**, 195115 (2020).
[34] K. M. Stadler, Ph.D. thesis, Ludwig-Maximilians-Universität München, 2019.
[35] D. Li, K. Lee, B. Y. Wang, M. Osada, S. Crossley, H. R. Lee, Y. Cui, Y. Hikita, and H. Y. Hwang, Nature (London) **572**, 624 (2019).
[36] M. Osada, B. Y. Wang, B. H. Goodge, K. Lee, H. Yoon, K. Sakuma, D. Li, M. Miura, L. F. Kourkoutis, and H. Y. Hwang, Nano Lett. **20**, 5735 (2020).
[37] K.-W. Lee and W. E. Pickett, Phys. Rev. B **70**, 165109 (2004).
[38] A. S. Botana and M. R. Norman, Phys. Rev. X **10**, 011024 (2020).
[39] Y. Nomura, M. Hirayama, T. Tadano, Y. Yoshimoto, K. Nakamura, and R. Arita, Phys. Rev. B **100**, 205138 (2019).
[40] H. Sakakibara, H. Usui, K. Suzuki, T. Kotani, H. Aoki, and K. Kuroki, Phys. Rev. Lett. **125**, 077003 (2020).
[41] M. Jiang, M. Berciu, and G. A. Sawatzky, Phys. Rev. Lett. **124**, 207004 (2020).
[42] X. Wu, D. Di Sante, T. Schwemmer, W. Hanke, H. Y. Hwang, S. Raghu, and R. Thomale, Phys. Rev. B **101**, 060504(R) (2020).
[43] M. Hepting, D. Li, C. Jia, H. Lu, E. Paris, Y. Tseng, X. Feng, M. Osada, E. Been, Y. Hikita *et al.*, Nat. Mater. **19**, 381 (2020).
[44] B. H. Goodge, D. Li, K. Lee, M. Osada, B. Y. Wang, G. A. Sawatzky, H. Y. Hwang, and L. F. Kourkoutis, Proc. Natl. Acad. Sci. U.S.A. **118**, e2007683118 (2021).
[45] S. Ryee, H. Yoon, T. J. Kim, M. Y. Jeong, and M. J. Han, Phys. Rev. B **101**, 064513 (2020).
[46] P. Jiang, L. Si, Z. Liao, and Z. Zhong, Phys. Rev. B **100**, 201106(R) (2019).
[47] L. Si, W. Xiao, J. Kaufmann, J. M. Tomczak, Y. Lu, Z. Zhong, and K. Held, Phys. Rev. Lett. **124**, 166402 (2020).
[48] P. Werner and S. Hoshino, Phys. Rev. B **101**, 041104(R) (2020).
[49] L.-H. Hu and C. Wu, Phys. Rev. Research **1**, 032046(R) (2019).
[50] Y.-H. Zhang and A. Vishwanath, Phys. Rev. Research **2**, 023112 (2020).
[51] P. Adhikary, S. Bandyopadhyay, T. Das, I. Dasgupta, and T. Saha-Dasgupta, Phys. Rev. B **102**, 100501(R) (2020).
[52] G.-M. Zhang, Y.-f. Yang, and F.-C. Zhang, Phys. Rev. B **101**, 020501(R) (2020).
[53] J. Gao, S. Peng, Z. Wang, C. Fang, and H. Weng, Natl. Sci. Rev. **09**, nwaa218 (2020).
[54] F. Bernardini, V. Olevano, and A. Cano, Phys. Rev. Research **2**, 013219 (2020).
[55] M.-Y. Choi, K.-W. Lee, and W. E. Pickett, Phys. Rev. B **101**, 020503(R) (2020).
[56] J. Karp, A. S. Botana, M. R. Norman, H. Park, M. Zingl, and A. Millis, Phys. Rev. X **10**, 021061 (2020).
[57] F. Lechermann, Phys. Rev. B **101**, 081110(R) (2020).
[58] V. Olevano, F. Bernardini, X. Blase, and A. Cano, Phys. Rev. B **101**, 161102(R) (2020).
[59] M. Kitatani, L. Si, O. Janson, R. Arita, Z. Zhong, and K. Held, npj Quantum Mater. **5**, 59 (2020).
[60] Y. Zhang, L.-F. Lin, W. Hu, A. Moreo, S. Dong, and E. Dagotto, Phys. Rev. B **102**, 195117 (2020).
[61] Q. Gu, Y. Li, S. Wan, H. Li, W. Guo, H. Yang, Q. Li, X. Zhu, X. Pan, Y. Nie *et al.*, Nat. Commun. **11**, 6027 (2020).
[62] X. Wu, K. Jiang, D. Di Sante, W. Hanke, J. Hu, and R. Thomale, arXiv:2008.06009.
[63] H. Zhang, L. Jin, S. Wang, B. Xi, X. Shi, F. Ye, and J.-W. Mei, Phys. Rev. Research **2**, 013214 (2020).
[64] F. Petocchi, V. Christiansson, F. Nilsson, F. Aryasetiawan, and P. Werner, Phys. Rev. X **10**, 041047 (2020).
[65] F. Lechermann, Phys. Rev. X **10**, 041002 (2020).
[66] Y. Wang, C.-J. Kang, H. Miao, and G. Kotliar, Phys. Rev. B **102**, 161118(R) (2020).
[67] C.-J. Kang and G. Kotliar, Phys. Rev. Lett. **126**, 127401 (2021).
[68] B. Kang, C. Melnick, P. Semon, S. Ryee, M. J. Han, G. Kotliar, and S. Choi, arXiv:2007.14610.
[69] X. Wan, V. Ivanov, G. Resta, I. Leonov, and S. Y. Savrasov, Phys. Rev. B **103**, 075123 (2021).
[70] M. Rossi, H. Lu, A. Nag, D. Li, M. Osada, K. Lee, B. Wang, S. Agrestini, M. Garcia-Fernandez, Y.-D. Chuang *et al.*, arXiv:2011.00595.
[71] D. Li, B. Y. Wang, K. Lee, S. P. Harvey, M. Osada, B. H. Goodge, L. F. Kourkoutis, and H. Y. Hwang, Phys. Rev. Lett. **125**, 027001 (2020).
[72] S. Zeng, C. S. Tang, X. Yin, C. Li, M. Li, Z. Huang, J. Hu, W. Liu, G. J. Omar, H. Jani *et al.*, Phys. Rev. Lett. **125**, 147003 (2020).
[73] H. U. R. Strand, Phys. Rev. B **90**, 155108 (2014).
[74] See Supplemental Material at http://link.aps.org/supplemental/10.1103/PhysRevLett.126.206401 for additional data and discussion, which includes Refs. [40,59,64,66,68,70,73,75,76].
[75] E. Pavarini, E. Koch, D. Vollhardt, and A. Lichtenstein, *The LDA+DMFT Approach to Strongly Correlated Materials, Reihe Modeling and Simulation*, Vol. 1 (Forschungszentrum Jülich, Jülich, 2011).
[76] L. Vaugier, H. Jiang, and S. Biermann, Phys. Rev. B **86**, 165105 (2012).
[77] P. W. Anderson, Phys. Rev. Lett. **34**, 953 (1975).
[78] H. Katayama-Yoshida and A. Zunger, Phys. Rev. Lett. **55**, 1618 (1985).
[79] C. M. Varma, Phys. Rev. Lett. **61**, 2713 (1988).
[80] A. Georges, G. Kotliar, W. Krauth, and M. J. Rozenberg, Rev. Mod. Phys. **68**, 13 (1996).
[81] S. Choi, P. Semon, B. Kang, A. Kutepov, and G. Kotliar, Comput. Phys. Commun. **244**, 277 (2019).
[82] E. Gull, A. J. Millis, A. I. Lichtenstein, A. N. Rubtsov, M. Troyer, and P. Werner, Rev. Mod. Phys. **83**, 349 (2011).
[83] I. Okada and K. Yosida, Prog. Theor. Phys. **49**, 1483 (1973).
[84] For the region of VS insulators, we found strong oscillations between $N = 2$ and $N = 4$ solutions at lower temperatures during DMFT iterations, and thus stable convergence was not achieved. However, the whole discussion of the present Letter is not affected by this limitation.
[85] J. R. Schrieffer and P. A. Wolff, Phys. Rev. **149**, 491 (1966).
[86] Y. Kuramoto, Eur. Phys. J. B **5**, 457 (1998).
[87] R. Micnas, J. Ranninger, and S. Robaszkiewicz, Rev. Mod. Phys. **62**, 113 (1990).
[88] $Z = [1 - \partial \mathrm{Im}\Sigma(i\omega_n)/\partial\omega_n|_{\omega_n \to +0}]^{-1}$, where $\Sigma(i\omega_n)$ is the fermionic self-energy on the Matsubara frequency axis. To

evaluate Z, we fitted the fourth-order polynomial to the lowest six Matsubara frequency $\Sigma(i\omega_n)$ following the strategy of Ref. [30].

[89] P. Cha, N. Wentzell, O. Parcollet, A. Georges, and E.-A. Kim, Proc. Natl. Acad. Sci. U.S.A. **117**, 18341 (2020).

[90] K. Steiner, S. Hoshino, Y. Nomura, and P. Werner, Phys. Rev. B **94**, 075107 (2016).

[91] S. Hoshino and P. Werner, Phys. Rev. B **93**, 155161 (2016).

[92] P. T. Dumitrescu, M. Serbyn, R. T. Scalettar, and A. Vishwanath, Phys. Rev. B **94**, 155127 (2016).

[93] J. P. Rodriguez and R. Melendrez, J. Phys. Commun. **2**, 105011 (2018).

[94] A. Subedi, O. E. Peil, and A. Georges, Phys. Rev. B **91**, 075128 (2015).

[95] P. Seth, O. E. Peil, L. Pourovskii, M. Betzinger, C. Friedrich, O. Parcollet, S. Biermann, F. Aryasetiawan, and A. Georges, Phys. Rev. B **96**, 205139 (2017).